Biased residuals of core flow models from satellite-derived 'virtual observatories'

Geophys. J. Int. (2009) **177,** 463–475 doi: 10.1111/j.1365-246X.2009.04111.x

Biased residuals of core flow models from satellite-derived 'virtual observatories'

C. D. Beggan,[1] K. A. Whaler[1] and S. Macmillan[2]

[1]*School of GeoSciences, University of Edinburgh,* EH9 3JW*, UK. E-mail: ciaran.beggan@ed.ac.uk*
[2]*British Geological Survey, Murchison House, Edinburgh,* EH9 3LA*, UK*

Accepted 2009 January 5. Received 2008 October 27; in original form 2008 August 19

SUMMARY

Large satellite vector data sets of the Earth's magnetic field have become available in recent years. Standard magnetic field models of the internal field are generated by parametrizing a small subset of these data through a least-squares spherical harmonic representation. An alternative approach is to create a set of 'virtual observatories' (VO) in space, mimicking the operation of fixed ground-based observatories. We derive VO data sets from both CHAMP and Ørsted satellite measurements. We calculate and directly invert the secular variation (SV) from these VO data sets, to infer flow along the core–mantle boundary using an L_1 (or Laplacian) norm method (to reduce the effect of outliers). By examining the residuals from the flow models, we find temporally and spatially varying biases and patterns in the vector components. We investigate potential causes for these patterns, for example, by selecting night-side only vector data and applying corrections to the input data, using external and toroidal fields calculated by Comprehensive Model 4 (CM4). We test the effect of a number of data selection and correction criteria and find evidence for influence from fields both internal and external to the satellite, orbital configuration and effects from the method of binning data to produce VO. The use of CM4 to correct the satellite data before calculating the VO SV grid removes a strong bias from external sources but, on average, does not greatly improve the fit of the flow to the data. We conclude that the best fit of the flows to the data is obtained using satellite night-side only data to generate VO. We suggest that, despite best efforts, external fields effects are not completely removed from SV data and hence create unrealistic secular acceleration.

Key words: Rapid time variations; Satellite magnetics; Planetary interiors.

1 INTRODUCTION

The Earth's large-scale magnetic field is believed to be generated and sustained by dynamo action within the fluid outer core (e.g. Christensen & Wicht 2007). The main field changes in both strength and direction over time, with the gradual variation termed the secular variation (SV). With certain assumptions, it is conjectured that flow at the core–mantle boundary can be inferred (subject to some uncertainty) from the SV observed at, or above, the surface of the planet. Since the mid-19th century, the strength and direction of the main field has been measured continuously at a limited number of fixed ground observatories, unevenly distributed across the globe (Bloxham *et al.* 1989). The last decade has seen a significant improvement in the capability to observe the global field at high spatial resolution. Several satellite missions have been launched, providing a rich new set of scalar and vector magnetic measurements, from which to model the global field and temporal variation in detail (Olsen *et al.* 2007). These new spatially comprehensive data sets complement the existing record of ground-based observatories. We exploit these new data to characterize the SV globally and attempt to improve upon the models of the core–boundary flow that have been constructed to date. We also use core flow modelling as a method to examine the effects of external field (and other influences) on models of the internal SV.

Using the approach developed by Mandea & Olsen (2006), we create sets of 648 'Virtual Observatories' (VO), distributed about the planet at 400 km above the Earth's surface, based upon satellite measurements from the CHAMP (Reigber *et al.* 2002) and Ørsted (Neubert *et al.* 2001) satellites over 5 yr (2001–2005). We invert the SV calculated at the VO for flow along the core–mantle boundary. Several previous studies have employed satellite data to recover core flows (Hulot *et al.* 2002; Holme & Olsen 2006), with recent results from Olsen & Mandea (2008) suggesting that rapidly varying flows may occur within the core.

In contrast to most other studies, we invert SV from vector data directly—rather than spherical harmonic model coefficients—to calculate flow model coefficients, permitting the incorporation of data uncertainties into the model. Direct comparison of the SV

generated by the flow model to the SV derived at individual VO can also be made, enabling the residuals to be investigated in detail. The results illustrate the difficulty of producing a completely internal SV model.

Section 2 of this paper outlines the processing of satellite data to derive the VO, whereas Section 3 summarizes the assumptions and method for flow inversion. In Section 4, we examine the patterns seen in the residuals between the SV produced by the flow model and the input SV. Section 5 assesses potential causes and explanations for these residual patterns whereas Section 6 suggests methods for ameliorating them.

2 VIRTUAL OBSERVATORIES

Ground-based observatories provide a high-quality temporal record of the magnetic field at a single point on the surface of the Earth. Observations are taken typically at 1 s intervals and made available in the form of minute, hourly, daily and monthly means. However, only a limited number of observatories are in simultaneous operation at any one time. The observatories are also unevenly distributed across the planet, with a large number concentrated in Europe and the Northern Hemisphere and a paucity in the Southern Hemisphere and Pacific Ocean region. Thus SV, as determined by ground observatories, is rather poorly constrained over large regions of the Earth.

Data from satellite missions (e.g. Magsat, Ørsted, CHAMP, SAC-C) have the advantage of sampling the magnetic field across almost the entire globe. However, depending on the orbital configuration, the revisit period for any particular point may be several days to months. This gives a poor temporal record for any specific region and hence comparison directly with ground-based observatory records is difficult. Previous studies have overcome this issue by parametrizing the field using a spherical harmonic representation and least-squares solving for a set of coefficients that best fit the data (Hulot *et al.* 2002; Lesur *et al.* 2008). This approach generates a set of spherical harmonic coefficients representing both the field and the SV, though these field models are created from a very small selection of quiet-time night-side data (Thomson & Lesur 2007). The CHAOS and xCHAOS field models (Olsen *et al.* 2006; Olsen & Mandea 2008) contain a larger subset of slightly noisier quiet time data (Kp index $\leq$ 2o) of satellite data from CHAMP, Ørsted and SAC-C. However, this still represents a vast under-utilisation of the available data.

2.1 VO Method

Mandea & Olsen (2006) suggested another method for treating the large volumes of data generated during the satellite missions. By binning and averaging all available satellite vector data within a cylinder of certain radius about a selected point into monthly time periods, they were able to match well the change in the magnetic field as recorded at ground observatories. As this approach attempts to mirror the method used for deriving monthly mean values for ground-based observatories, they refer to these points above the surface of the planet as 'virtual observatories'. A strong implicit assumption is that short-term external field effects will have a zero mean value over the period of a month.

To calculate the mean monthly field at a VO, the data must be reduced to a common height (due to the slightly elliptical and slowly decaying orbit of the satellite). Mandea & Olsen (2006) chose to bin data from a particular month within a cylinder of radius 400 km about the chosen latitude and longitude of the VO position. A main field model is subtracted from observed vector satellite data ($\boldsymbol{B}$) in the polar coordinate frame:

$$\Delta \boldsymbol{B} = \boldsymbol{B}^{\text{Satellite}} - \boldsymbol{B}^{\text{Main Field}}, \tag{1}$$

to produce a set of residual measurements $\Delta \boldsymbol{B}$, which are rotated into (x, y, z) Cartesian coordinates. It is assumed that the residual field can be represented as a Laplacian potential field $\Delta \boldsymbol{B} = -\nabla V$, which varies linearly in the local x, y and z Cartesian coordinate frame, with the origin in the centre of the cylinder (at 400 km altitude). This allows V to be calculated using eight independent parameters:

$$\begin{aligned} V = {} & v_x x + v_y y + v_z z \\ & + v_{xx} x^2 + v_{yy} y^2 - (v_{xx} + v_{yy}) z^2 \\ & + v_{xy} xy + v_{xz} xz + v_{yz} yz. \end{aligned} \tag{2}$$

These parameters $(v_x, v_y, \ldots, v_{yz})$ are estimated using a Huber robust least-squares method. The mean residual to the main field at the virtual observatory is thus $\Delta \boldsymbol{B} = -(v_x, v_y, v_z)$. The main field model at (r, θ, ϕ), where $r = 400$ km, is added back to the mean residual value to produce values of the North (X), East (Y) and Downward (Z) components of the field for a selected month. This procedure is repeated for all the available months in the data set at all VO locations.

The SV (or yearly change) at a given observatory for $month(t)$ is then calculated as the difference between the average field in $month(t-6)$ and $month(t+6)$ for the X, Y and Z components.

$$SV_{month(t)} = Field_{month(t+6)} - Field_{month(t-6)}. \tag{3}$$

This approach removes both the stationary crustal field component of the signal and the annual variation, without any direct filtering or averaging, giving the $\dot{X}$, $\dot{Y}$ and $\dot{Z}$ vector components of the field.

In their study, Mandea & Olsen (2006) found a strong correlation (for the period 2001.5–2005.5) between the SV observed at the Niemegk Observatory and the corresponding point at a height 400 km above Niemegk in the $\dot{X}$ and $\dot{Z}$ components (though no strong correlation was present in the $\dot{Y}$ component). Comparison of the SV at Niemegk and 21 other observatories to their respective VO values gave a mean correlation of $|\rho| = 0.65, 0.21, 0.73$ for the $\dot{X}$, $\dot{Y}$ and $\dot{Z}$ components, respectively.

Initially, for this study, corrected and calibrated CHAMP vector data were acquired from GFZ Potsdam (Level 2, 2007 Release v50) for the time period from 2001 May to 2005 December (56 months). Magnetic field series for 648 VO locations were calculated on two separate grids: (1) a regular grid of colatitude and longitude ($\theta = 5^\circ, 15^\circ, \ldots, 175^\circ$; $\phi = -180^\circ, -170^\circ, \ldots, 170^\circ$) mimicking the gridpoint arrangement of Mandea & Olsen (2006) and (2) an equal-area global grid of 648 tesserae (Leopardi 2006). At higher latitudes on the grid of equal latitude and longitude, data included in the VO cylinders are binned into more than one VO, as the areas overlap. At lower latitudes, there are gaps between the cylinders, meaning some data are not used. Using a grid of adjacent non-overlapping equal-area tesserae uses each measured datum just once in the calculation of the VO grid.

The CHAMP satellite samples the field at a frequency of 1Hz, giving over 86 000 points per day on average. The CHAOS model was used in eq. (1) as the main field model to compute the magnetic residuals. The 44 months of SV data and their standard deviations, from 2001 November to 2005 June, were then estimated using eq. (3).

3 FLOW MODELLING

Roberts & Scott (1965) examined the problem of determining fluid motions at the core–mantle boundary responsible for SV. However, many assumptions must be made to formulate the problem and reduce ambiguities in the resulting solutions. Deducing the flow velocity from SV is non-unique, even with perfect knowledge of the observed radial part of the field (B_r) and the SV ($\dot{B}_r$), as there are entire classes of flow that do not generate any detectable SV outside the core (Backus 1968).

3.1 Assumptions

Typically, the magnetic field lines are assumed fixed or 'frozen' relative to the core fluid motion over short periods of time (i.e. years to decades). This is known as the frozen-flux assumption (Alfvén 1942). On large scales (>1000 km), the magnetic diffusion (due to Ohmic decay) can be argued to operate on timescales of the order of 2×10^5 yr, so, can be ignored on timescales from years to decades. There are shortcomings to this approach, which are discussed in, for example, Gubbins & Kelly (1996), Gubbins (1996) and Love (1999). Backus (1968) devised a test of the frozen flux assumption but from examination of data from recent satellite missions, Holme & Olsen (2006) have suggested that it may not be possible to conduct the test conclusively.

Further assumptions must be made to produce a tractable problem. In particular, in most cases, the flow is truncated at a large spatial scale, and *a priori* constraints are imposed, giving a regularized solution via a damping (smoothing) parameter (Gubbins 1983; Madden & Le Mouël 1982; Bloxham *et al.* 1989). Assumptions about the type of flow at the core–mantle boundary are also required to reduce the inherent ambiguity. Examples include steady (Voorhies & Backus 1985), toroidal-only (Whaler 1980) or tangentially geostrophic (Hills 1979; Le Mouël 1984) flows, or flows with a particular helicity (Amit & Olson 2004). Recently, Pais & Jault (2008) have proposed large-scale quasi-geostrophic flow within the core. There are limits to the fidelity of the inverted flow models compared with the actual flows that generate the observed SV. A number of workers, including Rau *et al.* (2000) and Amit *et al.* (2007), have inverted artificial SV data generated from dynamo simulations to test how well flow inversion recovered the actual velocities and patterns. Their work suggests that it is possible to image correctly only the large spatial scale parts of the flow. However, despite the numerous shortcomings of the methods and data, generally consistent flow model solutions (using large-scale assumptions) are achieved from different data sets. In this sense, it may be possible to recover some aspects of the large-scale flow within the outer core. In this study, we are interested in examining the residuals to the flow and so have only imposed an assumption of tangential geostrophy upon the models.

3.2 One-norm iterative inversion

The inversion of observed SV data for a core flow model is undertaken with the use of a spectral spherical harmonic representation for the main field, SV, and the coefficients parametrizing the flow (Roberts & Scott 1965; Whaler 2007). As the horizontal velocity averages to zero over the core–mantle boundary, with the radial component across the boundary vanishing, the flow can be expressed in terms of poloidal (s) and toroidal (t) scalars expandable in spherical harmonics. These spherical harmonic coefficients, stored in a vector $\mathbf{m}$, are the flow model coefficients, whose values we seek using a regularized inversion approach.

Spherical harmonic SV coefficients can be ordered in a vector ($\dot{\mathbf{g}}$) and related to flow coefficients by

$$\dot{\mathbf{g}} = \mathbf{B}\mathbf{m}, \tag{4}$$

where $\mathbf{B}$ is the combined Elsasser and Gaunt matrix (Whaler 1986). The vector $\dot{\mathbf{g}}$ is related to surface and near-surface SV data, with $\mathbf{d} = \mathbf{Y}\dot{\mathbf{g}}$. The elements of the data vector, $\mathbf{d}$, are the VO SV components $\dot{X}$, $\dot{Y}$ and $\dot{Z}$. $\mathbf{Y}$ has elements that are multiples of spherical harmonics and their θ and ϕ derivatives. Thus, including the observational error ($\mathbf{e}$), the linear inverse problem becomes

$$\mathbf{d} = \mathbf{Y}\dot{\mathbf{g}} + \mathbf{e} = \mathbf{Y}\mathbf{B}\mathbf{m} + \mathbf{e} = \mathbf{A}\mathbf{m} + \mathbf{e} \tag{5}$$

We determine a solution by minimizing the size of the error vector using a particular measure or norm. The L_1 (or Laplacian) norm minimizes the absolute sum of the errors, compared with the standard L_2 formulation, which minimizes the sum of the squares. Errors in the measurement can often be correlated; so, a data covariance matrix, where the diagonal elements are the variances of the data, is used to capture this information.

To solve for $\mathbf{m}$ from the VO SV, a regularized inversion approach imposing large-scale assumptions is employed. The two-norm form (for Gaussian distributed uncertainties) of the solution is (Gubbins 1983):

$$\hat{\mathbf{m}} = (\mathbf{A}^T\mathbf{E}^{-1}\mathbf{A} + \lambda\mathbf{D})^{-1}\mathbf{A}^T\mathbf{E}^{-1}\mathbf{d}, \tag{6}$$

where $\mathbf{A}$ is the matrix of normal equations (from 5), $\mathbf{E}$ is the data covariance matrix and $\mathbf{d}$ is the data vector. $\mathbf{D}$ is the regularisation matrix, which can be used to incorporate *a priori* constraints, imposing a 'smoothness' (in this case, forcing the solution to be large scale) on the flow. Including $\mathbf{D}$ into the formulation is equivalent to minimizing a linear combination of the misfit norm and an initially defined solution norm (see Parker 1994, for a general discussion of such inverse problems). A damping parameter, λ, acts to control the importance attached to the data versus the imposition of a smooth flow. Regularisation also ensures numerical stability of the inversion and convergence of the expansion when the spherical harmonic series for $\mathbf{m}$ is truncated.

The minimisation of the L_2 norm provides adequate results. However, Walker & Jackson (2000) provide the motivation to compute flow models using an iterative L_1 norm minimisation method instead. We have observed that the residual fit of the SV generated by flow models to the data is generally Laplacian distributed, justifying the use of the Laplacian approach (Beggan & Whaler 2008). The minimisation of the L_1 norm has a number of advantages compared with the least-squares minimisation. In general, the influence of large outliers is reduced, and there is no requirement to implement data selection criteria prior to inversion (Farquharson & Oldenburg 1998).

In the L_1 algorithm, the residual differences from the previous iteration are used to form a diagonal matrix $\mathbf{R}_k$, whose elements are $\boldsymbol{R}_{ii} = \sqrt{2}/|e_i|$, where e_i is the residual of the ith datum at the kth iteration. $\mathbf{R}_k$ is re-calculated at each iteration. The iterative L_1 solution can be written as

$$\hat{\boldsymbol{m}}_{k+1} = \left(\mathbf{A}^T\mathbf{E}^T\mathbf{R}_k\mathbf{E}\mathbf{A} + \lambda\mathbf{D}\right)^{-1}\left(\mathbf{A}^T\mathbf{E}^T\mathbf{R}_k\mathbf{E}\,\mathbf{d}\right). \tag{7}$$

We apply the 'strong norm' of Bloxham (1988) as the *a priori* constraint in $\mathbf{D}$. This minimizes a global measure of the flow complexity (where u is the flow vector, ∇_h is the horizontal divergence

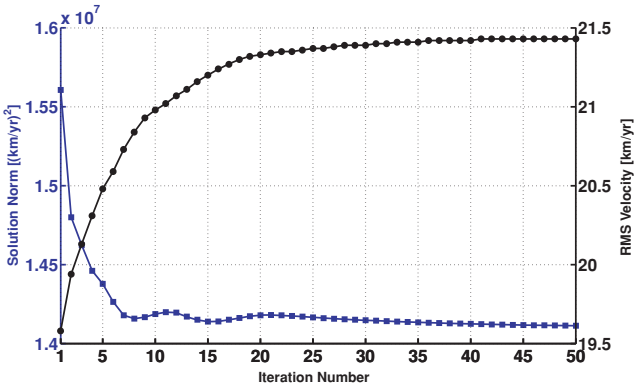

Figure 1. Convergence of the solution norm and root mean square velocity for flow model of 2005 March, using the L_1 iterative algorithm.

and l is the degree of truncation of the flow in the inversion):

$$\mathbf{m}^T\mathbf{D}\mathbf{m} = \oint_{\mathrm{CMB}} \left[\left(\nabla_h^2 u_\theta\right)^2 + \left(\nabla_h^2 u_\phi\right)^2\right] \mathrm{d}S$$
$$= 4\pi \sum_l \frac{l(l+1)^3}{2l+1} \sum_{m=0}^{l} \left[\left(t_l^m\right)^2 + \left(s_l^m\right)^2\right]. \quad (8)$$

Here t_l^m, s_l^m are coefficients of the spherical harmonic expansion of the poloidal and toroidal scalars. In this case, **D** is diagonal with elements $l(l+3)^3/(2l+1)$.

The CHAOS field model provides the main field coefficients for the Gaunt and Elsasser matrices (**B** in eq. 4). The standard deviation of the residual misfit from the estimate of data fit to the VO field in *month*$(t-6)$ and *month*$(t+6)$ is used to form the data covariance matrix. The residual errors for the first iteration of the L_1 solution are obtained from an initial starting model calculated by a two-norm solution (eq. 6) from the input data. The final solution of the one-norm iterative algorithm typically converges within 40 iterations (an example is shown in Fig. 1). We solve for flow coefficients up to degree and order $l = 14$. The value of very small ($<10^{-4}$) error residuals in the matrix **R** are set to 10^{-4} to prevent the formation of ill-conditioned matrices, as advocated by Walker & Jackson (2000). The damping parameter (λ) was set to 10^{-3} for all solutions. This produces solutions with different complexities (solution norm) but does not greatly affect the comparison between flow models. Note that there is no temporal smoothing of the flow.

The resulting flow model is used to predict the SV at each VO. The residual at the ith VO is $(d_i - \sum_j A_{ij}\hat{m}_j)$. Plotting the histogram of the residuals reveals how well fit the predicted SV generated by the flow model is to the input SV from the VO. A perfect fit of the model to the data would produce a histogram with a single peak at zero.

4 BIASED RESIDUALS

Following the example of Mandea & Olsen (2006) and Olsen & Mandea (2007), initially we exploited all the available CHAMP vector data from *all* local times over each month (for 56 months) to generate the global set of VO on a grid of equally spaced latitude and longitude. Each cylindrical VO 'bin' contained a large number (250 to 10 000) of points, depending on the data availability per month and generally increasing as a function of higher latitude (due to the polar orbit). Using eq. (3) to calculate the SV, we inverted the data set to derive a flow model for each month. In general, histograms of the residuals have a Laplacian distribution. The global distribution of residuals was expected to reveal a random pattern of positive and negative errors, but surprizingly, revealed biases, patterns and correlations between the $\dot{X}$, $\dot{Y}$ and $\dot{Z}$ components. Note that no temporal damping assumptions or constraints were imposed. Moreover, the distribution of the residuals in each component reveals more complex spatial patterns, with strong temporal variation.

It was observed that the pattern of modelled core flow changes significantly each month of the data set. Fig. 2 shows three examples of the instantaneous flow and associated residual histogram, and Fig. 3 shows the geographic distribution of the residuals for three separate months: 2001 November, 2003 February and 2005 March. In Figs 2(a), (c) and (e) the core flow models derived from the SV show large differences in flow patterns and are evidently influenced by a temporally changing signal in addition to the internal SV signal. The typical southern Indian Ocean gyre is present in all models; however, differences occur in the Northern Hemisphere and under western Eurasia. These month-to-month changes in flow are too large to be physically realistic.

The histograms of the residual fit of the SV generated by the flow model to the input data are shown in Figs 2(b), (d) and (f). An unbiased data set and flow inversion would be expected to produce an approximately zero-mean distribution of residuals. However, 2003 February has a significant negative skew with, arguably, a bimodal distribution (i.e. second peak at $-6\,\mathrm{nT\,yr^{-1}}$). 2005 March has the smallest skew of the three histograms, but has a non-zero mean, suggesting that some bias still exists.

The geographical distribution of the residuals in the $\dot{X}$, $\dot{Y}$ and $\dot{Z}$ components are shown in Fig. 3. Examination of the distribution in each component of the SV suggests that the $\dot{X}$ component is consistently the noisiest, whereas the $\dot{Z}$ component tends to have the smallest residuals. The residuals in the $\dot{X}$ component tend to be strongly biased—either positive or negative—whereas the $\dot{Y}$ and $\dot{Z}$ components have residuals with the opposite sign to $\dot{X}$ (i.e. inversely correlated). In general, the component biases balance to generate an approximately zero-mean Laplacian distribution histogram. For some months, hemispherical biases are evident, and often longitudinal 'bands' or 'stripes' of larger (or alternating sign) residuals occur (e.g. the $\dot{Y}$ components of Figs 3a and b). If viewed as a time-series, the longitudinal stripes can be seen to 'drift' or rotate consistently westwards by approximately 30° month^{-1}, matching the satellite orbital drift.

Fig. 4 shows examples of flow models from VO calculated using a grid of equal area tesserae. The flow models in Figs 4(a), (c) and (e) are similar to Fig. 2, indicating that the SV data from both gridding approaches are equivalent. The fit of the flow models to the data is slightly poorer in these examples (compare the histograms b, d, f in Figs 2 and 4). The residual distribution in Fig. 5 shows that the $\dot{X}$ component is still the noisiest. The $\dot{X}$ residuals in Fig. 5(b) reveal that the bias is strongest in mid-latitudes, with opposite signed residuals in either hemisphere of the $\dot{Z}$ component. The sectorial banding seen in the residual distributions for the equal latitude and longitude VO grid (e.g. Fig. 3b, $\dot{X}$) is less apparent. The polar regions appear less noisy (except in the $\dot{Z}$ component), presumably due to fewer points in these regions.

5 ANALYSIS

It is worth emphasizing that, in this study, core flow modelling is being employed as a method to study the consistency of the

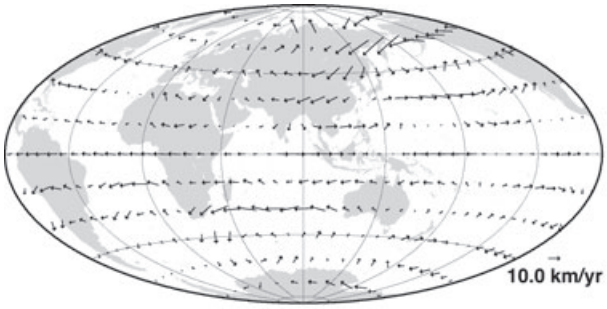

(a) Flow Model: November 2001

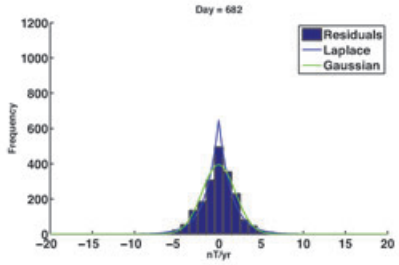

(b) Histogram of Flow Model Residuals: November 2001

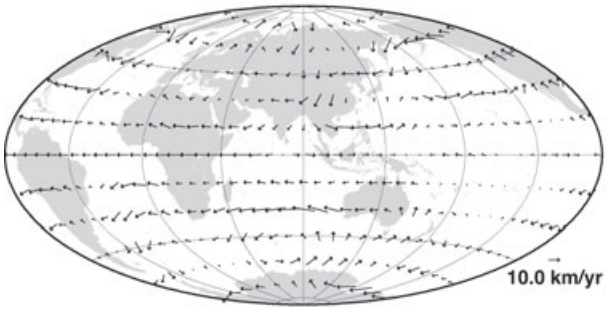

(c) Flow Model: February 2003

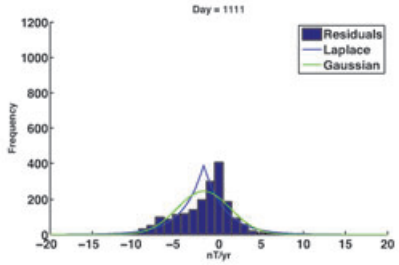

(d) Histogram of Flow Model Residuals: February 2003

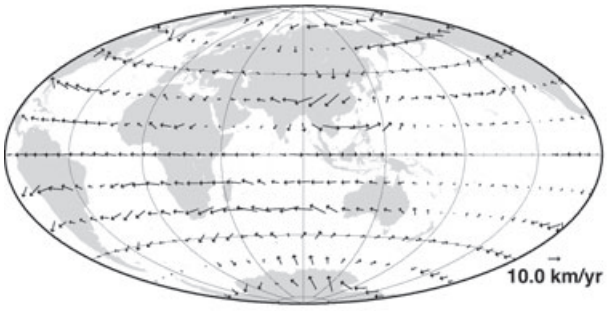

(e) Flow Model: March 2005

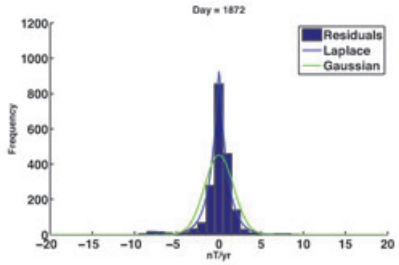

(f) Histogram of Flow Model Residuals: March 2005

Figure 2. Core–mantle boundary flow models, (a, c, e) and histograms (b, d, f) of residuals of each flow model to the SV generated from Virtual Observatory grid of equal latitude and longitude spacing for *all* available vector measurements. In (b, d, f), the Laplacian and Gaussian fit to the data are shown in the blue and green curves, respectively. Continents shown for reference.

internal SV deduced from satellite data, with the main aim being to understand and remove undesired effects. Analysis of the patterns in the residuals allows correction strategies to be developed.

Previous studies employing direct inversion of SV data from ground based observatories have not reported strong geographically biased vector components (e.g. Beggan & Whaler 2008); so, it is of interest to attempt to identify potential influences for the component biases and patterns seen, particularly the deviation from the implicit assumption of zero-mean noise. We wish to investigate if the residual bias results primarily from external or internal fields relative to the satellite, orbital drift or other effects.

To this end, a second set of main field VO for the period 2001 May–2005 December were calculated using local *night-side only* satellite data. The CHAMP vector data were winnowed to remove measurements outwith the local time window of 20.00–06.00hr (polar summer daylight conditions were ignored). The number of data in each cylindrical 'bin' (or tessera) was smaller (again dependent on the data availability during the particular month and latitude). Each month, approximately 5 per cent of the VO did not have enough data to calculate a solution, so, were spatially interpolated to fill the grid. As before, the SV for each VO was calculated and inverted for flow models for each month. We shall refer to this as VO Dataset 2, with the previous VO model using data from *all* local

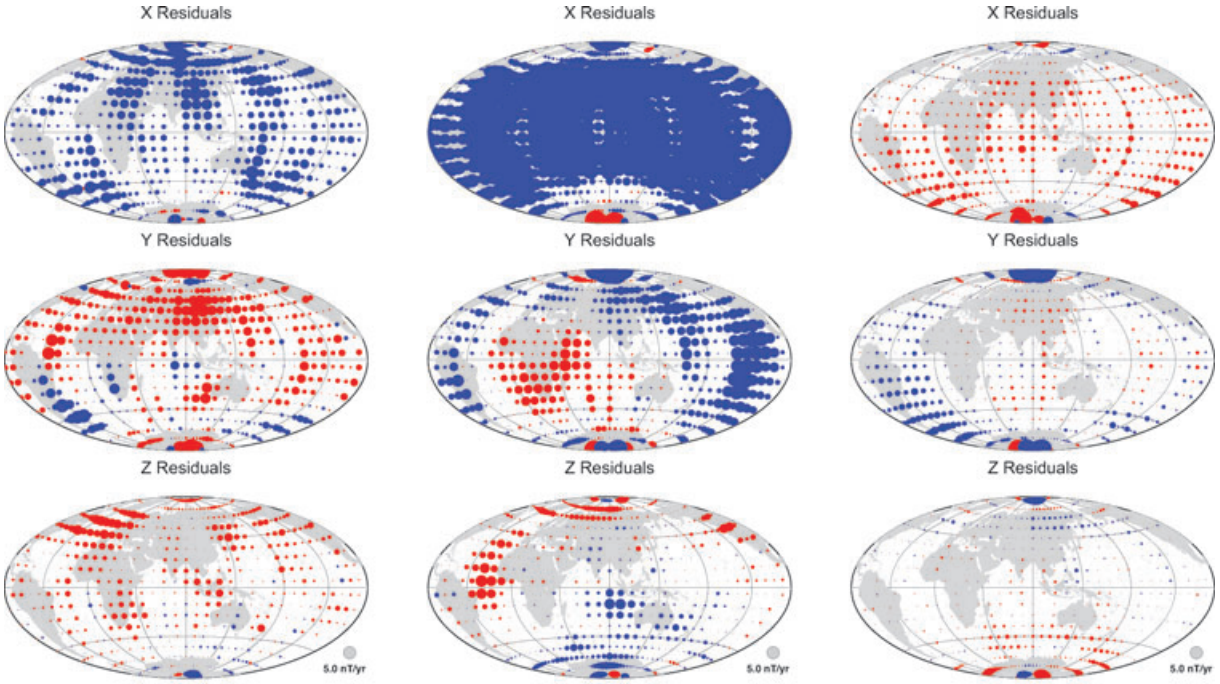

Figure 3. Geographic distribution of the residual fit of each flow model to the SV generated from Virtual Observatory grid of equal latitude and longitude spacing for *all* available vector measurements. Circle size indicates residual size, with reference circle shown in bottom right-hand panel. Positive residuals in red, negative residuals in blue.

times called Dataset 1 (Table 1 summarizes the data sets used in this study).

Comparison of residual histograms from this data set (not shown) with those from Dataset 1 indicates that the fit of the flow model to the SV data improves, illustrating that the night-side only data set is less perturbed. Fig. 6 shows three examples of the geographic residual patterns using the equally spaced latitude/longitude grid. The $\dot{X}$, $\dot{Y}$ and $\dot{Z}$ components are still strongly biased, with the longitudinal stripes particularly evident in Fig. 6(b). Note that overall the residuals for these flow models are smaller than those for Dataset 1 (e.g. compare Figs 3b and 6b).

5.1 Influence of fields external to satellite orbit

The previous results show that though some unwanted effects within the data collected on the day side of the planet can be reduced or removed, the biases in each vector component still remain. To examine the effects of external field influence on the residual biases and the sectorial banding, a data set of selected quiet-time data from Thomson & Lesur (2007) was used to generate a third VO data set (referred to as Dataset 3). The selection consists of vector data from both the CHAMP and Ørsted satellites for the same time period (2001 May–2005December), though due to the rigorous noise criteria imposed, has very few data points (approximately 85 000) compared with the previous CHAMP data sets. It was necessary to interpolate both spatially and temporally where lack of data prevented the calculation of an acceptable VO point. This is not ideal but is necessary to allow direct comparison to the other data sets.

With such strong initial selection criteria, there should be little temporal correlation in the data. Comparisons show that the SV calculated from this data set is reasonably consistent with the other two data sets. The SV was again inverted to produce instantaneous monthly flow models. Fig. 7 shows examples of the resulting residual patterns from three months with the lowest level of interpolation. There is no obvious banding or strong bias in any of the components, suggesting that external field noise (mostly absent in this data set) may affect the SV of VO generated using more relaxed data selection criteria.

External effects at satellite altitude come from a large number of phenomena including field aligned currents and ring currents. The Dst index measures magnetic disturbance from external fields, primarily due to ring current activity (Campbell 2003). Comparison between a nominal average monthly Dst value for 2001–2005 and the mean residual bias in the $\dot{X}$ component of Dataset 1 revealed no obvious correlation. However, as the SV is calculated using data measured 12 months apart, the correct manner of comparison is to compute the difference between the mean monthly Dst values for $month(t-6)$ and $month(t+6)$. Fig. 8 shows a strong correlation between the annual difference in mean monthly Dst value and the mean bias in the $\dot{X}$ component of Dataset 1 for both methods of gridding (as the actual flow model residuals are approximately zero-mean, the $\dot{Y}$ and $\dot{Z}$ component residuals are generally inversely correlated to those of the $\dot{X}$ component). The correlation is 0.67 for the equal area tesserae grid and 0.66 for the equally spaced latitude/longitude grid (both with a probability value of $\sim 10^{-7}$, indicating the correlation is significant at greater than the 99.9 per cent level). The significant correlations between the change in Dst and the two residual mean biases suggests that the residuals contain external field signals.

The VO data set created from selected quiet-time Ørsted and CHAMP measurements (Dataset 3) has been interpolated from a relatively small number of satellite data points both spatially and temporally. Hence, spatial correlation between measurements

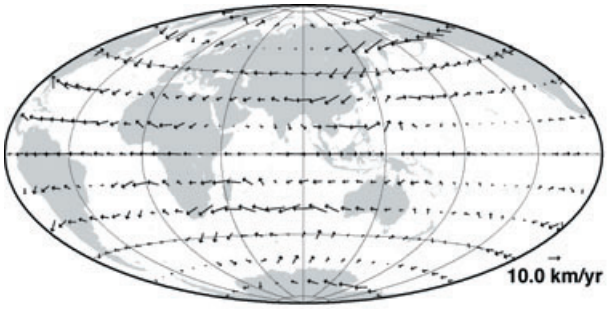

(a) Flow Model: November 2001

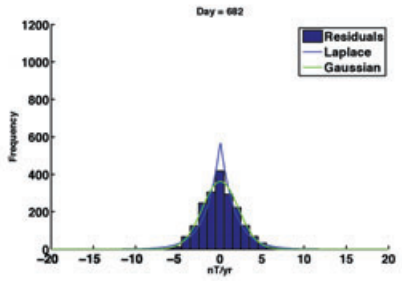

(b) Histogram of Flow Model Residuals: November 2001

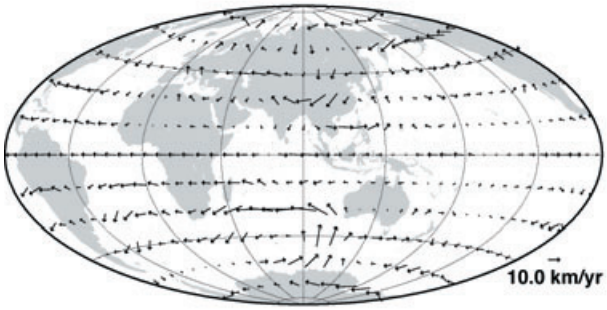

(c) Flow Model: February 2003

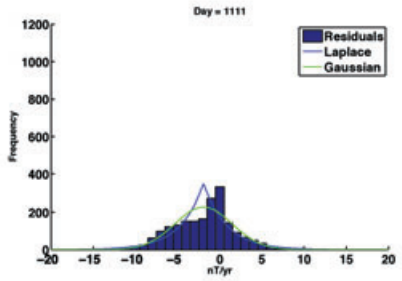

(d) Histogram of Flow Model Residuals: February 2003

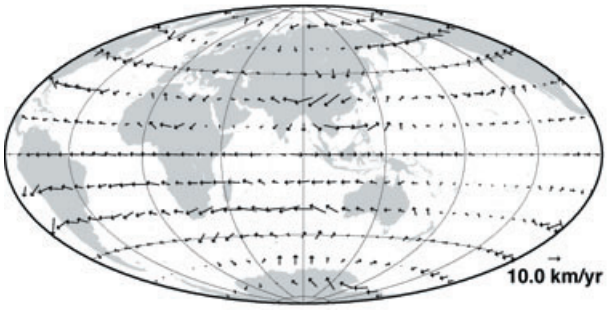

(e) Flow Model: March 2005

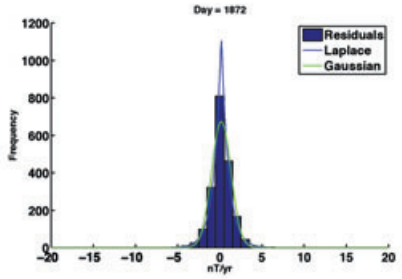

(f) Histogram of Flow Model Residuals: March 2005

Figure 4. Core–mantle boundary flow models (a, c, e) and histograms (b, d, f) of the residual fit of each flow model to the SV generated from Virtual Observatory data grid of equal area tessera for *all* available vector measurements. In (b, d, f), the Laplacian and Gaussian fit to the data are shown in the blue and green curves, respectively. Continents shown for reference.

is not as strong (though some correlation will exist due to interpolation). The associated residual patterns, shown in Fig. 7, do not have any of the features seen in those from Datasets 1 and 2; however, the correlation with the change in the Dst index is 0.49 (correlation is significant at greater than the 99.9 per cent level), which suggests that there is still some influence from external fields.

5.2 Influence of fields internal to satellite orbit

Magnetic fields internal to the satellite orbit (in addition to the main and crustal field) can arise from ionospheric currents, auroral/equatorial electrojets and field-aligned currents, particularly on the sunlit-side of each orbit—increasing globally during solar-disturbed periods. The additional fields would break the assumption that the field was of internal origin (i.e. a Laplace potential field) in the region surrounding the satellite as measurements are taken.

The smaller residuals from Dataset 2 (derived from night-side only measurements) compared with Dataset 1 (derived from all local-time measurements) suggest that there is a strong influence from day-side fields (e.g. Figs 3 and 6). Widening the window of local night-side measurements used in Datset 2 from 20.00–06.00 hr to 18.00–08.00 hr slightly increased the magnitude of the residuals. This suggests that ionospheric currents and other day-side fields are

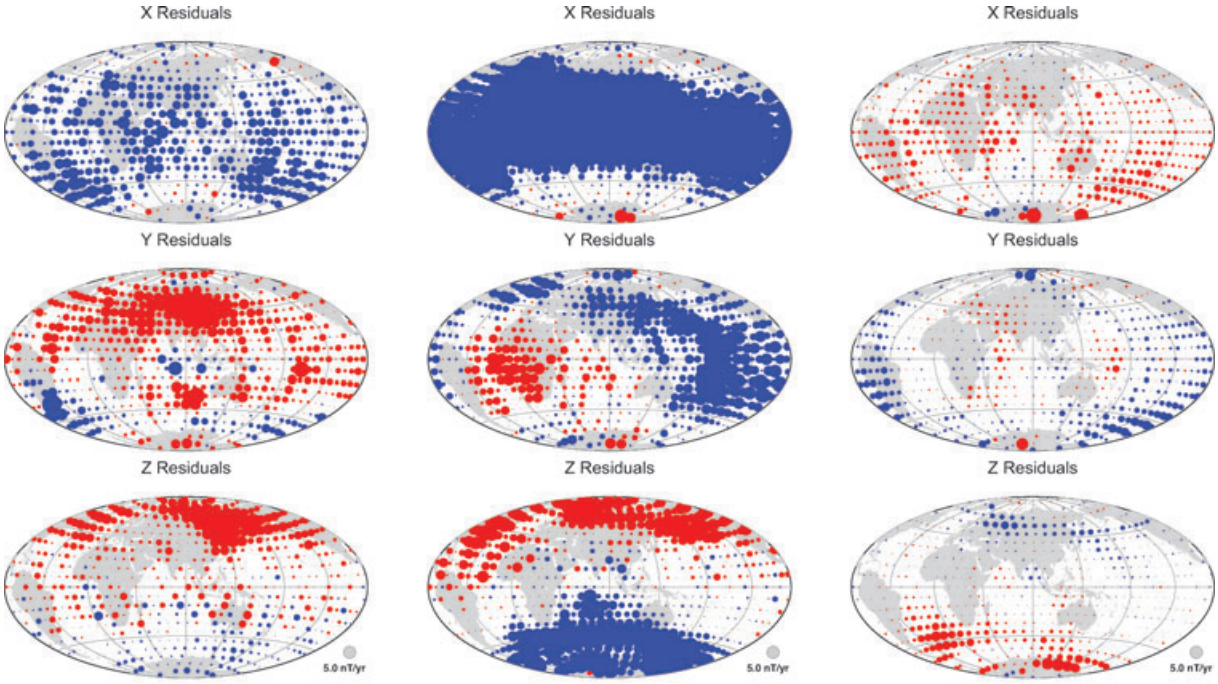

Figure 5. Geographic distribution of the residual fit of each flow model to the SV generated from Virtual Observatory data grid of equal area tessera for *all* available vector measurements. Circle size indicates residual size, with reference circle shown in bottom right-hand panel. Positive residuals in red, negative residuals in blue.

Table 1. Description of data sets generated for the study. Equal area refers to the grid of equal area tessera. Equal LL refers to a grid equally spaced in latitude and longitude.

Dataset	Characteristics	Gridtype
Dataset 1	All CHAMP data	Equal Area
	All CHAMP data plus CM4 correction	Equal LL
Dataset 2	Night-side only CHAMP data	Equal Area
	Night-side only CHAMP data plus CM4 correction	Equal LL
Dataset 3	Selected quiet-time CHAMP and Ørsted data	Equal LL
Dataset 4	Simulated CHAMP data using CHAOS	Equal LL

not averaged to zero by the VO method and hence contribute to the biased residuals.

5.3 Influence from the VO method

The method by which each VO is generated through binning and fitting a local potential field to produce an average field measurement over a month is, in part, responsible for some of the residual patterns observed. The cylindrical bin size, in the latitude/longitude grid, is fixed in radius (400 km); so, at higher latitudes, data measurements become common to several VO bins. The equal area tesserae grid does not have any overlapping regions and, so, removes these effects and uses all available observations. However, the fit of the flows using the equal area tessera method are, on average, slightly worse than those using the evenly spaced latitude/longitude grid.

The satellite nadir local-time difference also has an effect on the VO data. As the CHAMP satellite drifts approximately 2.5 hr month^{-1} in local time, measurements taken at dawn–dusk configurations are subject to a different ionospheric magnetic field environment to those acquired during local noon–midnight configurations. The difference of the median local satellite time (at mid-latitudes) between $month(t + 6)$ and $month(t - 6)$ is approximately 3.5 hr. Satellite measurements taken at different local times are not sampling the same magnetic field conditions.

As a test of orbital configuration influence (for the sectorial banding pattern, in particular), a synthetic VO data set (Dataset 4) was created using a simple satellite orbit simulator and the internal part of the CHAOS field model (Olsen *et al.* 2006). Two years of synthetic satellite measurements and positions were simulated by combining the CHAOS model and the latitude, longitude and radius output from the satellite simulation. The data were binned into 400 km cylinders on a regular grid of latitude and longitude to produce VO (similar to Fig. 2), providing 12 months of SV values, which were inverted for core flow models. A number of simple but unrealistic noise scenarios were tested using the simulation. Both biased (e.g. positive only) and unbiased random Gaussian noise was added to the CHAOS model in the polar regions and on the local dayside at low to mid latitudes, leaving other regions noise-free. Differing noise levels (up to 10 nT) have little effect on the size of the residuals and the pattern seen but do produce rapidly varying flow patterns, similar to the changes in the flows seen in the other data sets. Fig. 9 shows residual distributions for three consecutive months from the noise-free VO simulation. The residuals are seen to have persistent longitudinal banding features, which drift westward when viewed as a time-series. Residuals from a simulated

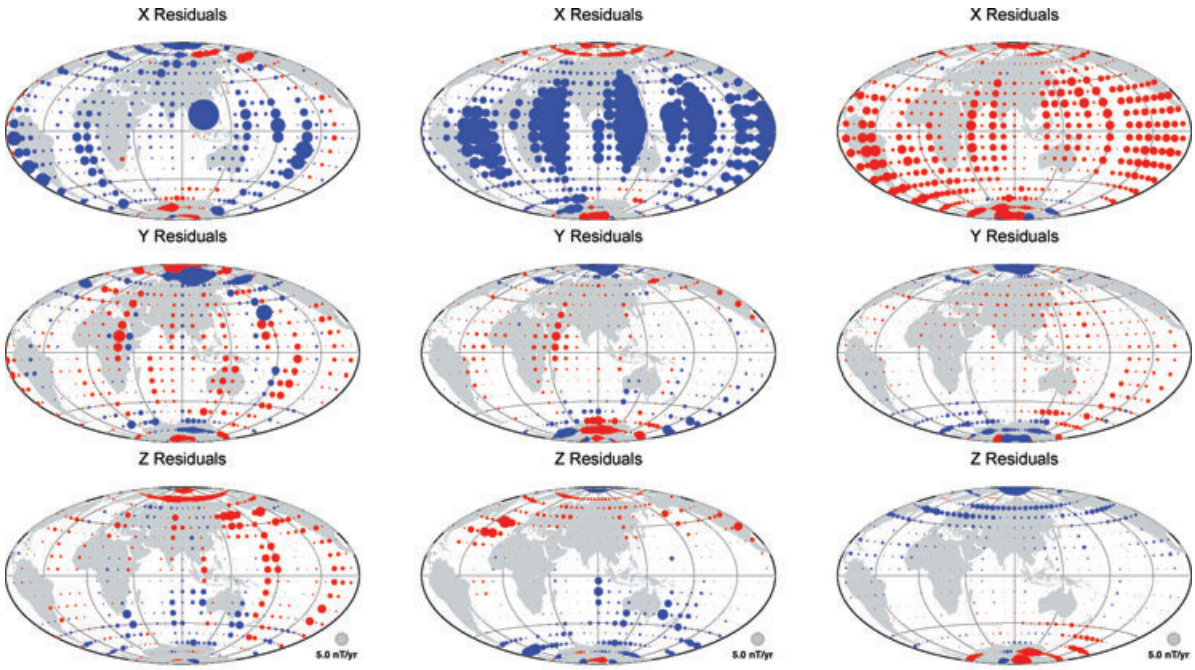

Figure 6. Geographic distribution of the residual fit of each flow model to the SV generated from Virtual Observatory grid of equal latitude and longitude spacing for *night-side only* vector measurements. Circle size indicates residual size, with reference circle shown in bottom right-hand panel. Positive residuals in red, negative residuals in blue.

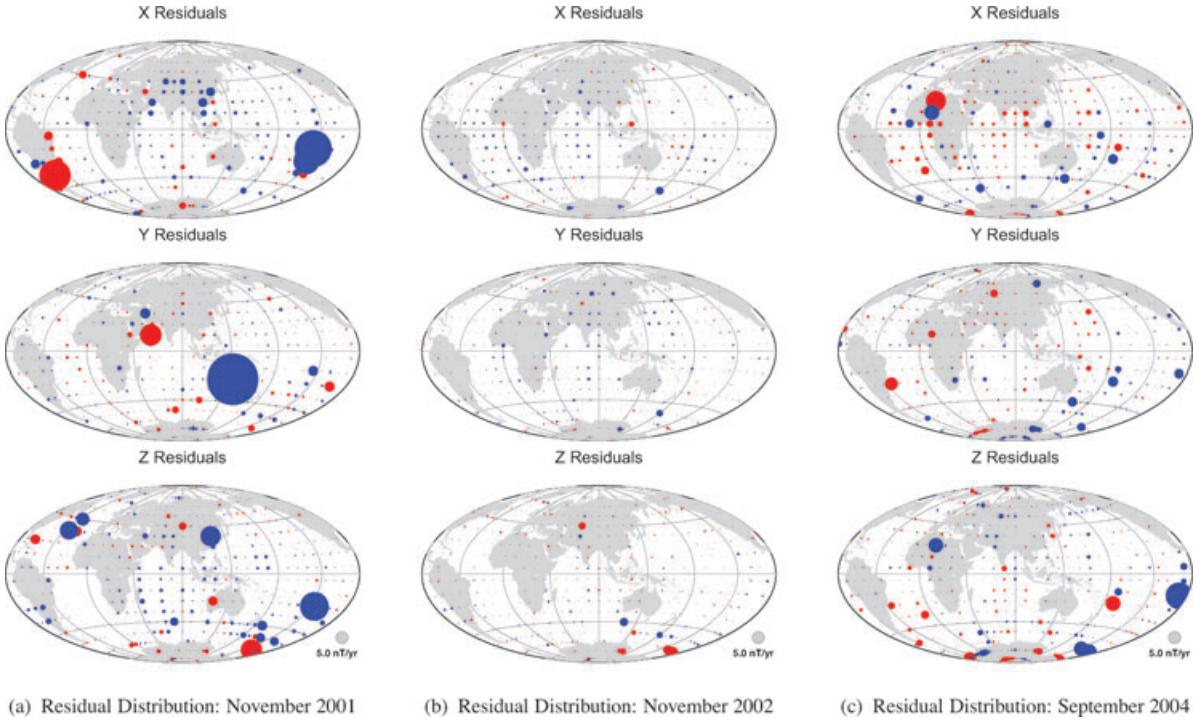

Figure 7. Geographic distribution of the residual fit of each flow model to the SV generated from Virtual Observatory grid of equal latitude and longitude spacing for *selected quiet-time* vector measurements (Dataset 3). Circle size indicates residual size, with reference circle shown in bottom right. Positive residuals in red, negative residuals in blue.

VO data set using a grid of equal area tessera show no latitudinal banding. This result demonstrates that the combination of binning method and orbital drift is at least partly responsible for the sectorial banding of the residuals.

6 CORRECTION STRATEGIES

In the previous section, we proposed and tested several causes for the biased residuals seen in Dataset 1 and Dataset 2. These include

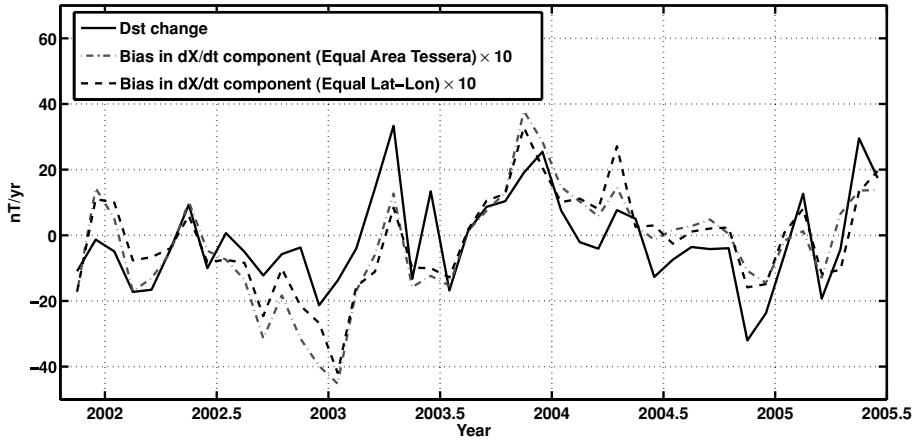

Figure 8. Twelve month difference of mean monthly Dst Index versus the mean bias in the $\dot{X}$ component residuals of Dataset 1 for the equal area tesserae VO grid and the equally spaced latitude/longitude VO grid. (Note: The biases have been multiplied by 10 to better illustrate the correlation). The correlation is 0.67 and 0.66, respectively (both correlations are significant at greater than the 99.9 per cent level).

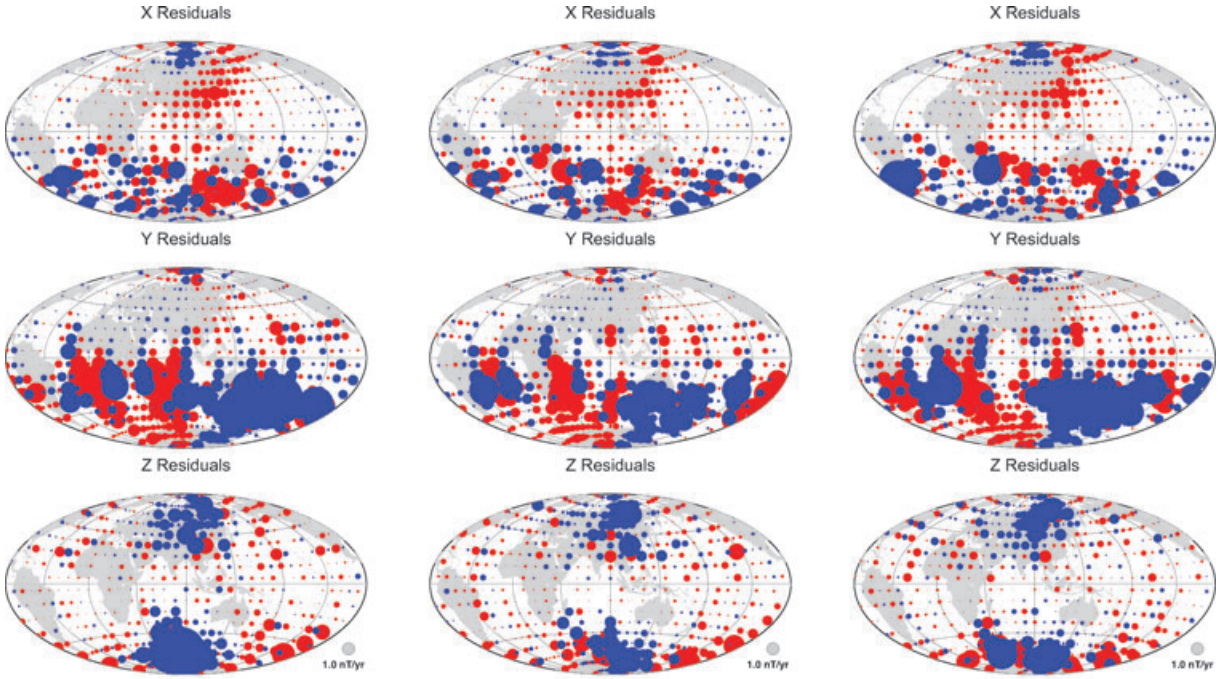

Figure 9. Geographic distribution of the residual fit of three flow models to SV data simulated from the CHAOS model and the CHAMP orbits generated from Virtual Observatory grid of equal latitude and longitude. Positive residuals in red, negative residuals in blue.

effects from (a) fields external to the satellite orbit, (b) fields internal to the satellite orbit but external to the Earth and (c) the orbital configuration of the satellite and the method of binning in preparation of the VO SV data sets. Here we analyse further the results of those tests, with the aim of removing or ameliorating the influence of these effects to produce data sets of purely internal SV, which are temporally consistent and spatially un-biased. At the same time, we must at least ensure that there is minimal 'aliasing' of undesirable effects into the SV data sets. These could manifest as unrealistic secular acceleration within the flow models. Olsen & Mandea (2008) have indicated that rapidly changing flows occur within the core but note, in the supplementary information for their paper, that these variations may in part be due to unmodelled external (ionospheric and magnetospheric) sources. They also clearly demonstrate in a previous study (Fig. 6 Olsen & Mandea 2007) that the first differences of the external and toroidal field Gauss coefficients (e.g. $\mathrm{d}q_1^0/\mathrm{d}t$ and $\mathrm{d}t_1^0/\mathrm{d}t$) are up to an order of magnitude larger than those for the coefficients for the internal SV. The calculations presented here strongly suggest that artefacts from external fields may affect their results.

6.1 Removal of fields using the comprehensive model

Modelling and removal of external, toroidal and induced magnetic fields at satellite altitude is complex. These magnetic fields have not been fully parametrized, nor can they be completely removed (Thomson & Lesur 2007). However, models of the external and other contributory magnetic fields, derived from parametrized

Table 2. Correlation between the mean bias of the $\dot{X}$ component of the residuals for each Dataset and the annual Dst difference.

	Dataset 1 (Equal LL)	Dataset 1 (Equal area)	Dataset 2 (Equal LL)	Dataset 2 (Equal area)
No correction	0.66	0.67	0.63	0.67
CM4 correction	0.41	0.42	0.10	0.16

inversion of large data sets, can be used to correct measured satellite data.

We tested the influence of removing external and ionospheric field models from the CHAMP satellite data using the Comprehensive Model (CM4) from Sabaka *et al.* (2004). The nominal hourly Dst index and the monthly F10.7 index over 2001–2006 were used as input parameters. The sum of the primary and secondary magnetospheric, ionospheric and toroidal fields were subtracted from the individual CHAMP measurements before binning and calculating the VO field. The resulting residuals from inverting for flow models showed mixed results compared with those from Dataset 1, but the corrected data did not, on average, produce a better fit (based on the sum of the absolute values of the residuals) than Dataset 2. However, this correction does reduce the correlation between the residual bias and the annual Dst difference (i.e. change in Dst Index). Table 2 shows the correlations between the annual Dst difference and the two VO data set residuals with two binning methods. This approach has the largest decorrelation effect on Dataset 2, where selected *night-side* only data are used, suggesting that the CM4 model performs better on the night-side of the planet (perhaps due to the less complex field environment).

However, correcting Dataset 2 using CM4 does not improve the overall fit of the flow to the data, as the size of the residuals remain approximately equal (for an equivalent solution norm). Fig. 10 shows the sum of the absolute values of the residuals (using the equal latitude/longitude binning method). Dataset 2 without CM4 correction provides the best overall fit to the data, though for some months (particularly towards the end of the data set), the CM4 corrected data sets are better. Individual comparison of the flow models between the CM4 corrected and uncorrected data sets show strong similarities. It would appear that CM4 removes much of the external part of the field and prevents most of it being aliased into the flow models, but introduces other unwanted signals, which reduces the effectiveness of the attempted correction.

6.2 Spherical harmonic analysis of the VO data sets

Rather than correcting the data individually, it might be possible to undertake a global correction of the VO field models. By applying spherical harmonic analysis to a VO field model, it is possible to separate the internal, external and toroidal field components (Olsen 1997). The individual components of the field (internal, external and toriodal) can be examined to understand how each distinct part contributes to the SV.

For each data set, the SV was resolved into its three components using the method of Olsen (1997). Each was then treated as if it were internal SV and inverted for instantaneous flow. The models of the flow generated by inverting internal SV, external SV or toroidal SV were examined in detail. All flow models showed rapid temporal variation.

The residual biases from the flow models inverted from the external component of the field were the most strongly correlated to the annual Dst difference. The geographic distribution of the residuals from the external component are similar to those observed in Datasets 1 and 2.

Examination of the residuals from flow models of the internal SV show that they are more randomly distributed than those from Datasets 1 and 2 (i.e. no patterns or $\dot{X}$, $\dot{Y}$ or $\dot{Z}$ component biases), suggesting that the biases arise mostly from the external and toriodal parts of the field. However, there is still a rapidly time varying component in the internal flow models, suggesting that some unwanted signal still remains within the internal flow model. This supports the assertion of Olsen & Mandea (2008) that isolating the internal SV is difficult.

The flow models from the toroidal and external parts of the SV have approximately 3.5 and 0.5 per cent of the root-mean-square flow velocity of the internal SV model. Although the internal flow coefficients represent most of the power in terms of root-mean-square velocity, they are not necessarily the source of all the variability in the flow from month to month. The individual contributions of the internal, external and toroidal components to the variability of the flow were examined. Table 3 shows the mean ratio of the standard deviation of the external and toroidal flow coefficients to the standard deviation of the internal flow coefficients. It was found that the combined variance of the external and toroidal components was similar to the variance of the internal coefficients. This suggests that the variability in the flow models from month to month comes approximately equally from the internal and the combined external and toroidal parts of the SV.

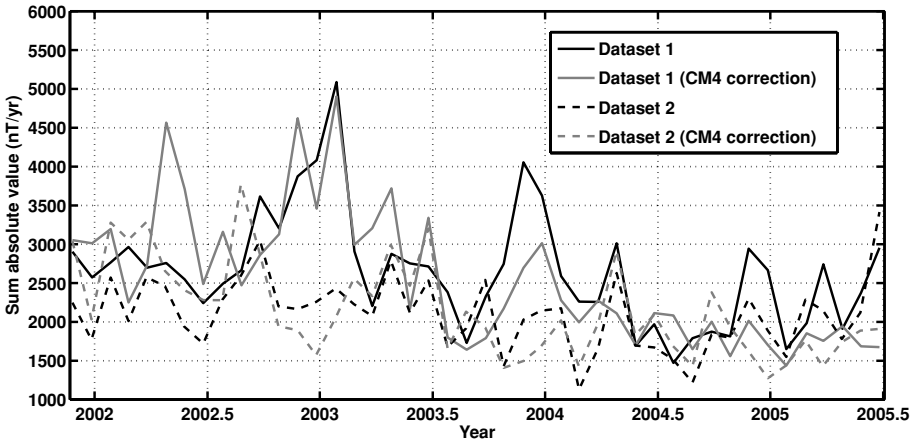

Figure 10. Comparison of the sum of absolute value of the residuals for Datasets 1 and 2 (grid of equal latitude/longitude) with and without external field correction using CM4. Note the solution norms are approximately similar.

Table 3. The mean ratio of the standard deviation of external and toroidal flow coefficients to the standard deviation of internal flow coefficients for the Equal Latitude/Longitude Datasets.

Dataset	Toroidal/Internal	External/Internal
Dataset 1: No correction	0.47	0.66
Dataset 1: CM4 correction	0.21	0.57
Dataset 2: No correction	0.40	0.23
Dataset 2: CM4 correction	0.28	0.41

7 CONCLUSION

The results from this study suggest that the assumption of Mandea & Olsen (2006) that the VO method produces zero mean, unbiased monthly field estimates is incorrect. The geographic distribution of the residuals to the flow models is strongly biased by external magnetic fields. When viewed in sequence, the flow models generated using all available CHAMP vector data (Dataset 1) show rapid variation in direction, strength and structure from month to month. The geographic distributions of the residuals also show continuous variation in component bias (from positive to negative), hemispherical bias, sectorial pattern and magnitude of bias.

There is a small improvement in the fit of the flows to the data when the night-side only vector data are used to create a VO data set (Dataset 2). A similar improvement can be seen when each satellite datum is corrected using a CM4 model to remove unwanted external and internal (to the satellite) fields prior to binning. This points to magnetospheric, ionospheric and day-side current systems as a significant source of contamination. In contrast, the smaller, more randomly distributed residuals from the selected quiet-time Ørsted-CHAMP data (Dataset 3) indicate that contamination of these data is much less, though still present. This points to signals external to the satellite orbit contaminating Datasets 1 and 2.

Another potential source of non-zero mean error is the method of generating the VO data set. The CHAMP satellite precesses approximately 2.5 hr month^{-1} in local time. As the data used to generate the VO are not from all local times, rather a small subset of day/night local times, this has the effect of *not* averaging out diurnal effects. For example, in a month where the local time is noon on the day side and midnight on the night side, a significant bias must be present due to currents internal to the satellite orbit. As noted in eq. (3), to calculate the annual SV for a particular month the VO value for 6 months prior is subtracted from the VO value 6 months ahead. The magnetic field environment will also be different for measurements collected 12 months apart, as the satellite nadir local times vary between 3 and 5 hr due to orbital drift. For example, a VO with a predominantly noon local time subtracted from a VO with predominantly morning local time will sense different ionospheric related fields. A grid with equal latitude/longitude spacing, where bins overlap near the poles and have gaps between them at the low latitudes, rather than equal area tessera, was found to accentuate certain patterns, such as sectorial banding and predominance of large residuals at the polar regions. The results from a synthetic data set support the conclusion that sectorial banding is related to the orbital drift and binning method.

Separation of the SV into its internal, external and toroidal components partitioned most of the influence from external sources into the external part of the SV, as expected. However, the flow models inverted from the internal component of the VO SV data set still retained a rapidly varying signal, indicating that isolation of the purely internal field is difficult.

In conclusion, unwanted signals from a number of sources have been identified in the field models derived from employing the VO method. Some of the effects from these sources can be removed or ameliorated, through the selective use of data, external field modelling and alternative binning approaches. Using a grid of equal latitude/longitude with local night-side only data selection (Dataset 2), best isolates the internal SV and reduces the influence from other sources but accentuates sectorial banding of the residuals. However, it appears that the VO data sets are influenced by unmodelled sources from fields other than the main field. These external influences appear to be responsible for the rapidly changing core flows.

ACKNOWLEDGMENTS

We wish to thank Nils Olsen for his advice, for code and for providing certain CHAMP data. We also thank Alan Thomson for the provision of Ørsted and CHAMP satellite data. The CHAMP data used in this study were supplied by GFZ Potsdam. We thank reviewers Nicolas Gillet and Monica Korte for helping improve the initial manuscript. This research is part of the NERC GEOSPACE programme, funded under grants NER/O/S/2003/00674 and NER/O/S/2003/00677. CDB is funded under NERC studentship award NER/S/J/2005/13496. This paper is published with the permission of the Executive Director of the BGS (NERC).

REFERENCES

Alfvén, H., 1942. On the existence of electromagnetic-hydrodynamic waves, *Nature,* **150,** 405–406.

Amit, H. & Olson, P., 2004. Helical core flow from geomagnetic secular variation, *Phys. Earth planet. Int.,* **147,** 1–25.

Amit, H., Olson, P. & Christensen, U., 2007. Tests of core flow imaging methods with numerical dynamos, *Geophys. J. Int.,* **168,** 27–39.

Backus, G.E., 1968. Kinematics of geomagnetic secular variation in a perfectly conducting core, *Phil. Trans. R. Soc. Lond. A,* **263,** 239–266.

Beggan, C. & Whaler, K., 2008. Core flow modelling assumptions, *Phys. Earth planet. Inter.,* **167,** 217–222.

Bloxham, J., 1988. The determination of fluid flow at the core surface from geomagnetic observations (Chap. 9), in *Mathematical Geophysics*, pp. 189–208, D. Reidel Publishing Company, Dordrecht.

Bloxham, J., Gubbins, D. & Jackson, A., 1989. Geomagnetic secular variation, *Phil. Trans. R. Soc. Lond.,* **329**(1606), 415–502.

Campbell, W., 2003. *Introduction to Geomagnetic Fields*, 2nd edn, Cambridge University Press, Cambridge.

Christensen, U. & Wicht, J., 2007. *Treatise on Geophysics*, Vol. 8, pp. 254–282, Numerical dynamo simulations, Elsevier, Amsterdam.

Farquharson, C.G. & Oldenburg, D.W., 1998. Non-linear inversion using general measures of data misfit and model structure, *Geophys. J. Int.,* **134,** 213–227.

Gubbins, D., 1983. Geomagnetic field analysis—I. Stochastic inversion, *Geophys. J. R. astr. Soc.,* **73,** 641–652.

Gubbins, D., 1996. A formalism for the inversion of geomagnetic data for core motions with diffusion, *Phys. Earth. planet. Sci.,* **98,** 193–206.

Gubbins, D. & Kelly, P., 1996. A difficulty with using the frozen flux hypothesis to find steady core motions, *Geophys. Res. Lett.,* **23**(14), 1825–1828.

Hills, R., 1979. Convection in the Eath's mantle due to viscous shear at the core-mantle interface and due to large-scale bouyancy, *PhD thesis*, N.M. State University, Las Cruces.

Holme, R. & Olsen, N., 2006. Core surface flow modelling from high-resolution secular variation, *Geophys. J. Int.,* **166,** 518–528.

Hulot, G., Eymin, C., Langlais, B., Mandea, M. & Olsen, N., 2002. Small-scale structure of the geodynamo inferred from Oersted and Magsat satellite data, *Nature,* **416,** 620–623.

LeMouël, J.-L., 1984. Outer-core geostrophic flow and secular variation of Earth's geomagnetic field, *Nature,* **311,** 734–735.

Leopardi, P., 2006. A partition of the unit sphere into regions of equal area and small diameter, *Electron. Trans. Numer. Anal.,* **25,** 309–327.

Lesur, V., Wardinski, I., Rother, M. & Mandea, M., 2008. GRIMM: the GFZ Reference Internal Magnetic Model based on vector satellite and observatory data, *Geophys. J. Int.,* **173,** 382–394.

Love, J., 1999. A critique of frozen-flux inverse modelling of a nearly steady geodynamo, *Geophys. J. Int.,* **138,** 353–365.

Madden, T. & Le Mouël, J.-L., 1982. The recent secular variation and motions at the core surface, *Phil. Trans. R. Soc. A,* **306,** 271–280.

Mandea, M. & Olsen, N., 2006. A new approach to directly determine the secular variation from magnetic satellite observations, *Geophys. Res. Lett.,* **33**(15), L15306.

Neubert, T. *et al.*, 2001. Oersted satellite captures high-precision geomagnetic field data, *EOS, Trans. Am. geophys. Un.,* **82**(7), 87–88.

Olsen, N., 1997. Ionospheric F region currents at middle and low latitudes estimated from Magsat data, *J. geophys. Res.,* **102**(A3), 4563–4576.

Olsen, N. & Mandea, M., 2007. Investigation of a secular variation impulse using satellite data: the 2003 geomagnetic jerk, *Earth planet. Sci. Lett.,* **255,** 94–105.

Olsen, N. & Mandea, M., 2008. Rapidly changing flows in the Earth's core, *Nature Geoscience,* **1,** 390–394.

Olsen, N., Lühr, H., Sabaka, T., Mandea, M., Rother, M. & Toffner-Clausen, L., 2006. CHAOS: a model of the Earth's magnetic field derived from CHAMP, Oersted, and SAC-C magnetic satellite data, *Geophys. J. Int.,* **166,** 67–75.

Olsen, N., Hulot, G. & Sabaka, T., 2007. The present field, in *Treatise on Geophysics*, Vol. 5, pp. 33–75, Elsevier, Amsterdam.

Pais, M. & Jault, D., 2008. Quasi-geostrophic flows responsible for the secular variation of the Earth's magnetic field, *Geophys. J. Int.,* **173,** 421–443.

Parker, R.L., 1994. *Geophysical Inverse Theory*, Princeton University Press, Princeton.

Rau, S., Christensen, U., Jackson, A. & Wicht, J., 2000. Core flow inversion tested with numerical dynamo models, *Geophys. J. Int.,* **141,** 485–497.

Reigber, C., Lühr, H. & Schwintzer, P., 2002. CHAMP mission status, *Adv. Space Res.,* **30,** 129–134.

Roberts, P. & Scott, S., 1965. On the analysis of the secular variation. 1. A hydromagnetic constraint: theory, *J. Geomag. Geoelec.,* **17,** 137–151.

Sabaka, T., Olsen, N. & Purucker, M., 2004. Extending comprehensive models of the Earth's magnetic field with Oersted and CHAMP data, *Geophys. J. Int.,* **159,** 521–547.

Thomson, A. & Lesur, V., 2007. An improved geomagnetic data selection algorithm for global geomagnetic field modelling, *Geophys. J. Int.,* **169,** 951–963.

Voorhies, C. & Backus, G., 1985. Steady flows at the top of the core from geomagnetic field models: the steady motion theorem, *Geophys. Astrophys. Fluid Dyn.,* **32,** 163–173.

Walker, M. & Jackson, A., 2000. Robust modelling of the Earth's magnetic field, *Geophys. J. Int.,* **143-3,** 799–808.

Whaler, K., 1980. Does the whole of the Earth's core convect?, *Nature,* **287,** 528–530.

Whaler, K.A., 1986. Geomagnetic evidence for fluid upwelling at the core-mantle boundary, *Geophys. J. R. astr. Soc.,* **86,** 563–588.

Whaler, K.A., 2007. Core Motions, in *Encyclopedia of Geomagnetism and Paleomagnetism*, pp. 84–89, Springer, Dordrecht.